2006

A Dynamic Simulation Model for Fan-and-Damper Controlled Refrigerators

Christian J. L. Hermes
Multibras S.A. Eletrodomesticos

Claudio Melo
Federal University of Santa Catarina

A Dynamic Simulation Model for Fan-and-Damper Controlled Refrigerators

Christian J. L. HERMES[1], Cláudio MELO[2]

[1] Multibrás S.A. Eletrodomésticos, Corresponding Author
Dona Francisca St., #7200, 89219-901 Joinville, SC, BRAZIL
Phone: +55 47 34 41 49 81 email: chermes@multibras.com.br

[2] Department of Mechanical Engineering, Federal University of Santa Catarina
P.O. Box 476, 88040-900 Florianópolis, SC, BRAZIL
Phone: +55 48 32 34 56 91 email: melo@polo.ufsc.br

ABSTRACT

A first-principles model for simulating the dynamic behavior of household refrigerators is presented herein. The model is used to simulate a typical Brazilian 440-litre top-mount refrigerator, in which the compressor is on-off controlled by the freezer temperature, while a thermo-mechanical damper is used to set the fresh-food compartment temperature. Innovative modeling approaches are proposed for each of the refrigerator components. Numerical predictions are compared to experimental data showing a reasonable level of agreement for the whole range of operating conditions, including the start-up and cycling regimes. The system energy consumption was found to be within ±10% agreement with the experimental data, while the air temperatures of the compartments were predicted with a maximum deviation of ±1°C.

1. INTRODUCTION

A household refrigerator is basically composed of a thermally insulated cabinet and a refrigeration loop, as illustrated in Fig.1. Its performance is usually evaluated by one of the following approaches (i) simplified calculations based on component characteristic curves; (ii) numerical analyses via commercial CFD packages; and (iii) standardized experiments. Although the first two techniques play important roles in component design, they do not provide enough information about component matching and system behavior, which is only obtained by testing the refrigerator in a controlled environment chamber. However, such tests are time consuming and expensive.

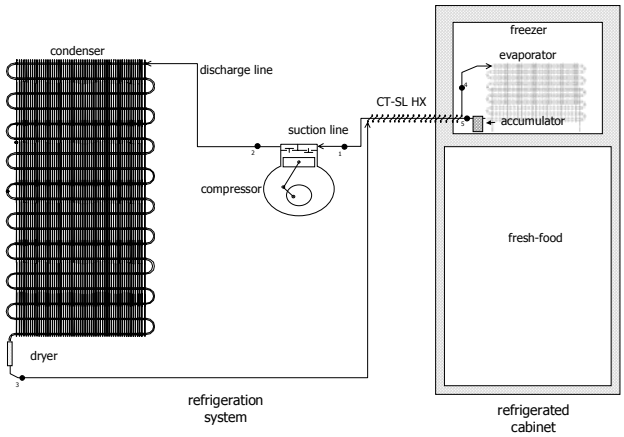

Figure 1: Schematic of a top-mount refrigerator

A faster and less costly alternative is the use of first-principle models for simulating the thermal- and fluid-dynamic behaviour of refrigeration systems. Steady-state and dynamic approaches can both be used. While the first is mainly used for component matching, the second is essential to define the controlling strategies and to optimize the system performance. Former dynamic models for refrigeration systems date back to the early 80s and were mostly focused on heat pump systems (Chi & Didion 1982, Yasuda et al. 1983, MacArthur 1984). The development of dynamic models for household refrigerators was stimulated by the CFC-12 phase-out in the late 80s (Melo et al. 1988, Jansen et al. 1988). Very few approaches available in the literature (Jakobsen 1995, Ploug-Sørensen 1997) are able to simulate the cycle behavior of household refrigerators, and none of them have been properly validated against experimental data on energy consumption. The development and validation of a model to estimate the energy consumption of household refrigerators is therefore the main focus of this study.

2. MATHEMATICAL MODELING

The overall system modeling requires the development of sub-models for each of the cycle components, which are summarized below. Detailed information can be found in Hermes (2006).

2.1 Heat Exchangers: Condenser and Evaporator

The model for refrigerant flow through the condenser and evaporator coils relies on the following simplifying assumptions: (i) 1D flow; (ii) straight, horizontal and constant cross-sectional tubes; (iii) negligible diffusion effects; and (iv) negligible pressure drop. The governing equations, derived from the mass and energy conservation principles applied to each of the control volumes (CV) illustrated in Fig.2, are given below:

$$V_k\dot{\rho}_k + w_k - w_{k-1} = 0 \quad ; \quad V_k\left(u_k\dot{\rho}_k + \rho_k\dot{u}_k\right) + w_k h_k - w_{k-1}h_{k-1} = \overline{Q}_k \tag{1}$$

where an upwind scheme was used to average the flow properties, and the averaged heat transfer term was integrated using the trapezoidal rule.

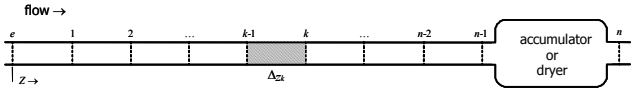

Figure 2: Diagram of the finite-volume discretization of the heat exchanger coil

As the refrigerant pressure through the coil is constant, the set of 2*n* dynamic ordinary differential equations ODEs may be re-organized into a set of *n*+1 linear equations (Rossi & Braun 1999), with *n* equations for the internal energy time-derivatives and 1 equation for the *dp/dt* term as follows:

$$\begin{bmatrix} V_1(\rho_1 - p\,\phi_1/\rho_1) & 0 & 0 & 0 & -V_1 p\dfrac{\psi_1}{\rho_1} \\ -\Delta h_1 V_1\phi_1 & V_2(\rho_2 - p\,\phi_2/\rho_2) & 0 & 0 & -V_2 p\dfrac{\psi_2}{\rho_2} - \Delta h_2 V_1\psi_1 \\ \vdots & \vdots & \ddots & 0 & \vdots \\ -\Delta h_1 V_1\phi_1 & -\Delta h_2 V_2\phi_2 & \cdots & V_n(\rho_n - p\,\phi_n/\rho_n) & -V_n p\dfrac{\psi_n}{\rho_n} - \Delta h_n\displaystyle\sum_{j=1}^{n-1} V_j\psi_j \\ V_1\phi_1 & V_2\phi_2 & \cdots & V_n\phi_n & \displaystyle\sum_{j=1}^{n} V_j\psi_j \end{bmatrix} \begin{Bmatrix} \dot{u}_1 \\ \dot{u}_2 \\ \vdots \\ \dot{u}_n \\ \dot{p} \end{Bmatrix} = \begin{Bmatrix} \overline{Q}_1 - w_e\Delta h_1 \\ \overline{Q}_2 - w_e\Delta h_2 \\ \vdots \\ \overline{Q}_n - w_e\Delta h_n \\ w_e - w_n \end{Bmatrix} \tag{2}$$

where $\phi = (\partial\rho/\partial u)_p$ and $\psi = (\partial\rho/\partial p)_u$. The peculiar shape of the coefficient matrix, with the lower band and the last row (*n*+1) terms different from zero, permits its analytical inversion by LU-decomposition. Such an approach not only reduces the number of ODEs, but also provides an explicit and evolving equation for pressure calculation.

The refrigerant properties were calculated in advance by the REFPROP 7 software and stored in the computer memory in the form of cubic splines. Gnielinski's (1976) correlation was used to estimate the single-phase flow heat transfer coefficients, while Jung's et al. (2003) and Wongwises' et al. (2000) correlations were adopted to estimate the condensing and evaporating heat transfer coefficients, respectively. The void fraction models proposed by Baroczy (1965) and Yashar et al. (2001) were used to estimate the refrigerant mass in the condensing and evaporating regions, respectively.

The heat exchanger sub-model takes into account the heat transfer between fins and tubes and between the internal and external fluid streams. The following simplifying assumptions were considered: (i) negligible heat conduction in the tube; (ii) one CV per tube (Domanski, 1991); and (iii) fin efficiency calculated by Schmidt's (1945) procedure. The wall temperature of the *k*-th tube, shown in Fig.2, is then given by:

$$\dot{T}_{w,k} = \left[A_i\hbar_r\left(T_{r,k} - T_{w,k}\right) + \left(A_t + \eta_f A_f\right)\hbar_a\left(T_{a,k} - T_{w,k}\right)\right]\left[c_w\left(M_t + \eta_f M_f\right)\right]^{-1} \tag{3}$$

The airflow through the evaporator has been modeled as quasi-steady, neglecting the presence of moisture. The evaporator air temperature was obtained from an energy balance, also considering the tube-by-tube approach:

$$T_{a,k} = \left\{\left[w_a c_{p_a} - \tfrac{1}{2}\hbar_a\left(A_t + \eta_f A_f\right)\right]T_{a,k-1} + \hbar_a\left(A_t + \eta_f A_f\right)T_{w,k}\right\}\left[w_a c_{p_a} + \tfrac{1}{2}\hbar_a\left(A_t + \eta_f A_f\right)\right]^{-1} \tag{4}$$

where the airside heat transfer coefficients are calculated by a correlation derived from experimental data (Hermes, 2006):

$$Nu = 0.125\,Re_{max}^{0.654}\cdot Pr^{1/3} \tag{5}$$

where *Nu* refers to the tube outer diameter and Re_{max} to the air velocity at the minimum free flow area. The condenser is a natural draft wire-on-tube heat exchanger, where the airside temperature was assumed uniform and constant. The airside heat transfer coefficients are calculated by a dimensionless correlation derived from experimental data (Hermes, 2006):

$$\pi_0 = 0.231\pi_1^{0.102}\pi_2^{0.631}\pi_3^{-0.259}\pi_4^{0.453}\pi_5^{0.616}\pi_6^{0.079} \tag{6}$$

$$\pi_0 = \hbar_c/\hbar_r + 1 \;\; ; \;\; \pi_1 = A_t/A_{tot} \;\; ; \;\; \pi_2 = A_f/A_{tot} \;\; ; \;\; \pi_3 = p_t/d_t - 1 \pi_4 = p_f/d_f - 1 \;\; ; \;\; \pi_5 = L_t/d_t \;\; ; \;\; \pi_6 = T_w/T_a - 1$$

Figure 3 compares the measured heat transfer rates to those calculated by equations (5) and (6). As can be seen, the proposed correlations are able to predict the experimental data within an error band of ±10%.

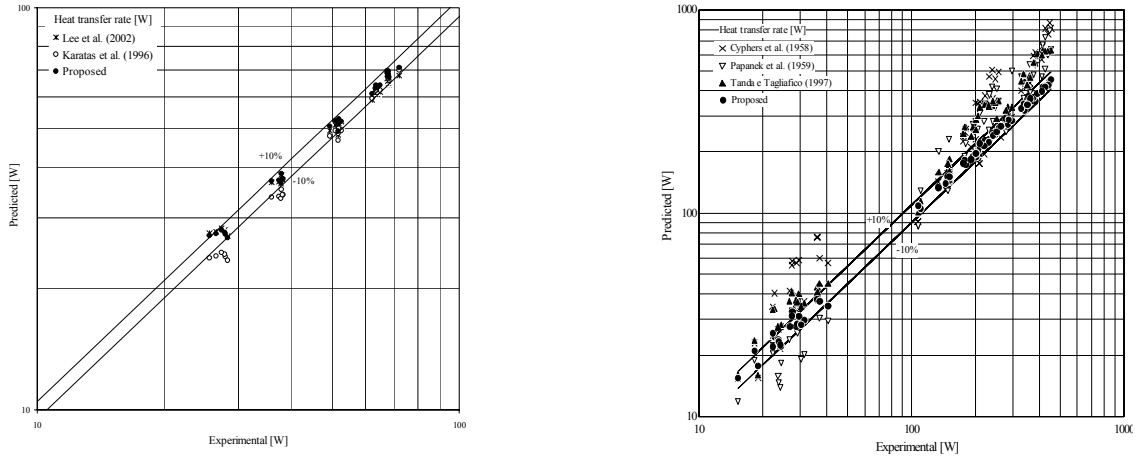

Figure 3: Proposed airside heat transfer correlations: finned-tube evaporators (*l*); wire-on-tube condensers (*r*)

2.2 Capillary Tube-Suction Line Heat Exchanger (CT-SL HX)

The CT-SL HX sub-model is based on the following simplifying assumptions: (i) 1D, viscous, compressible, homogeneous, and quasi-steady flow; (ii) negligible diffusion effects; (iii) negligible heat conduction in the tube walls ; (iv) straight, horizontal and constant cross-sectional area tube; (v) negligible pressure drops at the tube inlet and outlet; and (vi) negligible metastable flow effects. The refrigerant flow through the capillary tube is governed by the mass, energy and momentum principles, which provide the following set of differential equations, in the pressure domain:

$$dl/dp = -\Delta^{-1}\left[1 + G^2\left(\Phi v + \Psi\right)\right] \qquad ; \qquad dh/dp = -\Delta^{-1}\left[\tau\left(G^2 v\Psi\right) + qG^{-1}\left(1 + G^2\Psi\right)\right] \tag{7}$$

where $\Delta = \tau\left(1 + G^2 v\Phi\right) + qG\Phi$, $\Phi = \left(\partial v/\partial h\right)_p$, $\Psi = \left(\partial v/\partial p\right)_h$. From these equations the tube length and refrigerant enthalpy are calculated as a function of the pressure drop in any flow region. As there is no explicit equation for the mass flow rate, its calculation follows an iterative procedure governed by the calculated and actual tube lengths. The boundary conditions are the pressure and enthalpy at the inlet of the capillary tube and the exit pressure. The critical pressure was calculated according to Fauske's (1962) criterion, in which $dl/dp \rightarrow 0$ at the capillary tube exit. The differential equations (7) have been successfully solved by Heun's scheme (2nd order) using a grid with 50 integration points.

The suction line model is based on the following simplifying assumptions: (i) flow of only superheated vapor along the suction line; (ii) no heat transfer to the surroundings; and (iii) negligible pressure drop. From such assumptions the suction line outlet temperature is estimated by means of the heat exchanger effectiveness, avoiding the use of an additional iterative loop. A correlation for the CT-SL HX effectiveness was obtained from a comprehensive experimental database for HFC-134a and HC-600a. Such a correlation predicts the experimental data with a maximum deviation of ±10% (Fig. 4*l*). The CT-SL HX model predictions were compared with more than 1000 experimental data points for adiabatic and non-adiabatic flows of HFC-134a and HC-600a (see Fig.4*r*). As can be seen the experimental data are reasonably predicted by the model, with 85% of all data points falling within a ±10% error band.

2.3 Reciprocating Compressor

The compressor sub-model was divided into two domains: compressor shell and compression process (see Fig.5). The first allows the calculation of the refrigerant mass flow rate at the compressor inlet using a balance between the refrigerant mass flow rate discharged into the condenser and the amount of refrigerant absorbed/released from the lubricating oil, which is given by

$$w_o = -M_o\, \dot{\sigma}/dt/\left(1 - \sigma\right)^2 \tag{8}$$

If $d\sigma/dt > 0$ then $w_o < 0$, meaning that the refrigerant is absorbed by the oil. The opposite scenario is observed when $d\sigma/dt < 0$. Both discharged mass flow rate and compression power are calculated by the compression process model,

based on mass and energy balances within the cylinder (Prata et al., 1994). The following additional assumptions are taken into account: (i) homogeneous properties and an adiabatic process within the cylinder; (ii) suction and discharge valves modeled as two-position elements (fully-open and fully-closed); (iii) valve dynamics are neglected; (iv) effective flow areas are approximated by the orifice cross-sectional areas.

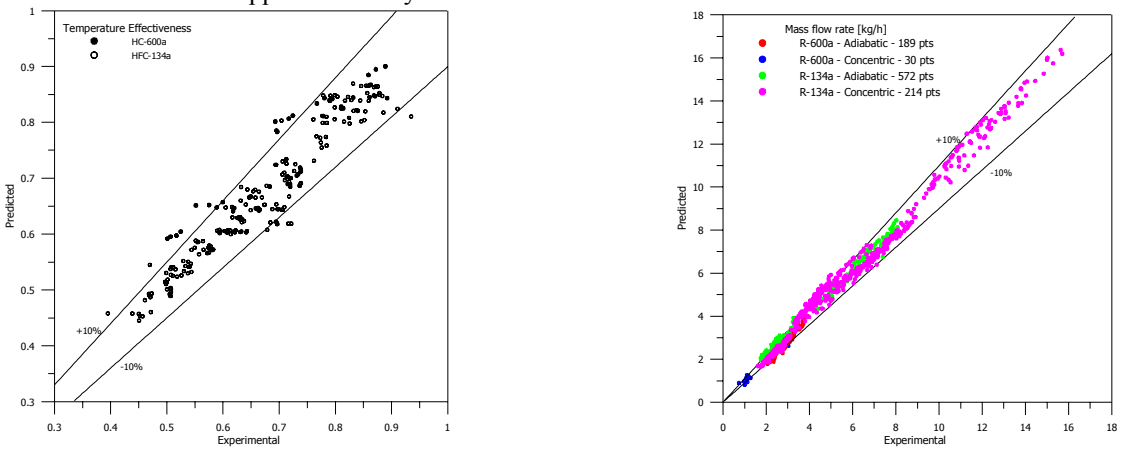

Figure 4: CT-SL HX sub-model validation: effectiveness correlation (*l*); mass flow rate predictions (*r*)

The set of differential equations for the compression process is solved at each time-step by a 1st order scheme, using an exponential interpolation and a grid with 360 nodes. Figure 6 compares the model predictions for the discharged refrigerant mass flow rate (*l*) and compression power (*r*) from calorimeter data. A linear behavior between calculated and measured values was identified, expressed by the following pair of correction functions:

$$w_d^{corr} = 0.942 w_d - 0.469 \quad ; \quad W_c^{corr} = 1.315 W_c + 11.2 \tag{9}$$

where w_d is expressed in [kg/h] and W_c in [W]. It should be noted that only two data points are required to extend the model to other compressor models.

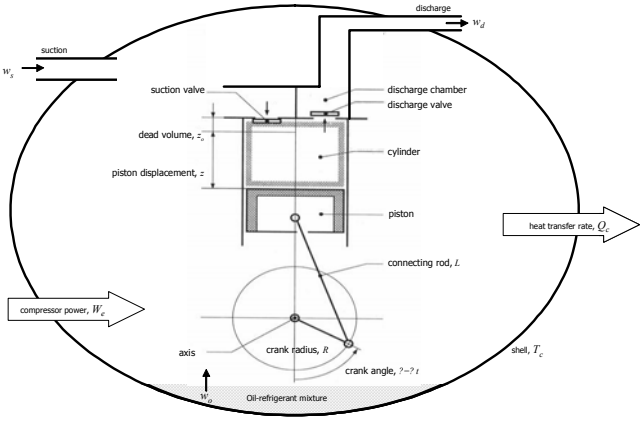

Figure 5: Schematic of the compressor sub-model

2.4 Refrigerated Compartments

The cabinet walls are modeled according to a 1D finite-volume scheme (Fig.7*l*). The temperature at each *k*-th wall layer is given by

$$\dot{T}_k = \alpha_w \left(T_{k+1} + T_{k-1} - 2T_k \right) / \Delta n \tag{10}$$

The wall thickness were considered uniform for both compartments (fresh-food and freezer). Equivalent thicknesses were determined from a reverse heat leakage test, taking into account not only the heat transmission through the walls, but also the heat gains in the gasket region. The insulation density was corrected to conserve the overall mass of the wall. The airside thermal resistances were neglected, and therefore the internal air and the inner liner temperatures are considered to be the same,

$$\dot{T}_i = \left[w_i c_p \left(T_{in} - T_i \right) + 2 k_{PU} A_{si} \left(T_w^{k=N} - T_i \right) / \Delta n + \dot{Q}_{gen} \right] \left[C_{si} + M c_p \left(T_a / T_i \right) \right]^{-1} \tag{11}$$

The airflow rates supplied to each compartment were measured in a wind-tunnel test facility (Hermes, 2006), as a function of the damper position (see Fig.7*l*).

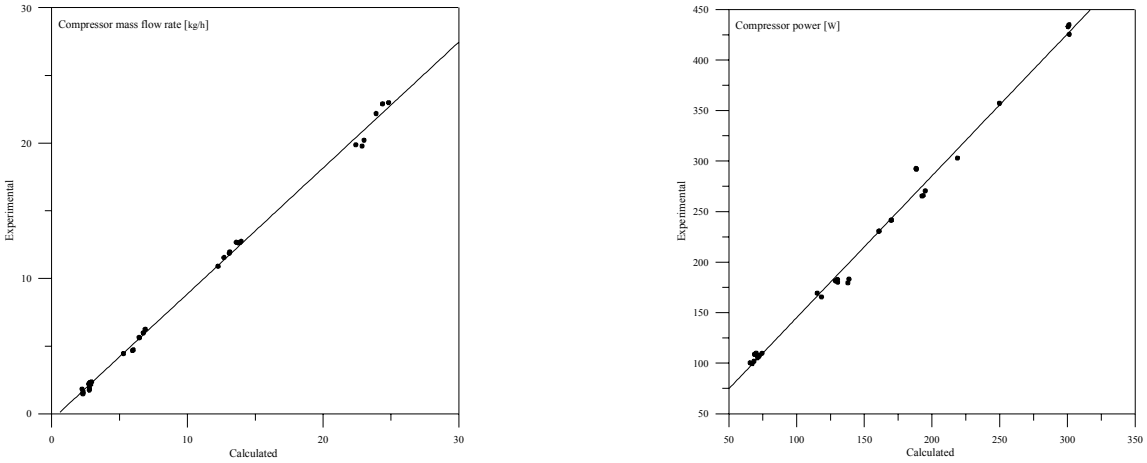

Figure 6: Linear correction functions for the compressor sub-model: mass flow rate (*l*); compression power (*r*)

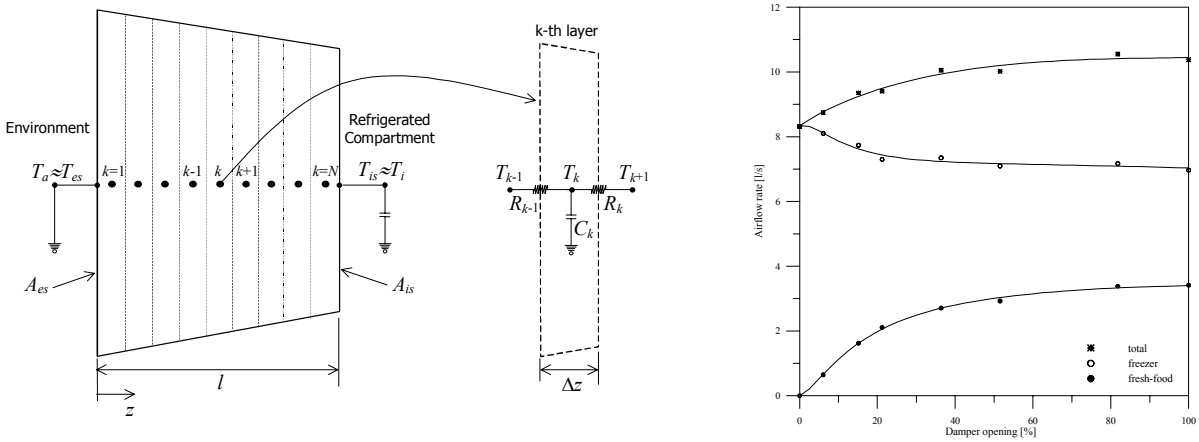

Figure 7: Finite-volume discretization of cabinet walls (*l*); airflow as a function of damper position (*r*)

2.5 Numerical Methodology

Two different time-scales can be observed in the refrigerator dynamics. The fastest is related to the refrigerant mass migration from one component to another, taking just a few minutes to reach the steady-state condition. The slowest relates to the cabinet thermal inertia and consequently the rate of heat transfer to the evaporator, taking hours to stabilize. One may notice that the first is inherent to the refrigeration system ODEs, while the second is linked to the cabinet ODEs. This behavior has encouraged a solution involving the segregation of the cabinet and system dynamic ODEs: solving the first by an explicit 1st order method, and integrating the second using the Adams predictor-corrector method, with both order and step size controllers. The cycle components are coupled to each other by the mass flow rate-enthalpy pair, and are transported from one component to another according to the refrigerant flow direction (Fig.1). The model requires only two initial conditions: ambient temperature (32°C) and refrigerant charge (85g, HFC134a). The equalizing pressure is internally calculated by the model.

3. MODEL VALIDATION

Tests with the refrigerator were carried out in an environmental chamber, in which both air temperature (32°C±0.5°C) and relative humidity (50%±5%) were controlled. Table 1 compares the experimental data with model predictions under the steady-state condition, showing maximum deviations of ±1°C and ±5% for the air temperatures and compressor power, respectively. Figure 8 shows the time variation of the air temperatures (*l*) and compressor power (*r*) during the start-up, with the damper at the maximum cooling position. It can be seen that the model is able to estimate the pull-down time and the compressor power with a maximum deviation of ±4% and ±5%, respectively.

Table 2 compares the model predictions with experimental data in terms of energy consumption, running factor, and air temperatures. The four control limits were considered (thermostat-damper): MAX-MAX, MAX-MIN, MIN-MAX, MIN-MIN. It can be observed that the model is able to predict the overall energy consumption and the

average air temperatures with maximum deviations of ±10% and ±1°C, respectively. The effect of the control limits on the predicted average air temperatures is better illustrated by a control-chart (Fig.9*l*). Fig.9*r* illustrates the suction and discharge pressure profiles through a typical cycle with the controls at the MAX-MAX position. It can be seen that the numerical results are in close agreement with the experiment data.

Table 1: Steady-state model validation

Damper	Fresh-food compartment temperature [°C]			Freezer compartment temperature [°C]			Compressor power [W]		
	Exp.	Sim.	Diff.	Exp.	Sim.	Diff.	Exp.	Sim.	Diff.
MAX	1.6	1.7	+0.1	-28.0	-27.7	+0.3	106.4	108.7	-2.2%
MIN	9.8	10.8	+1.0	-29.7	-28.7	+1.0	101.2	105.7	+4.4%

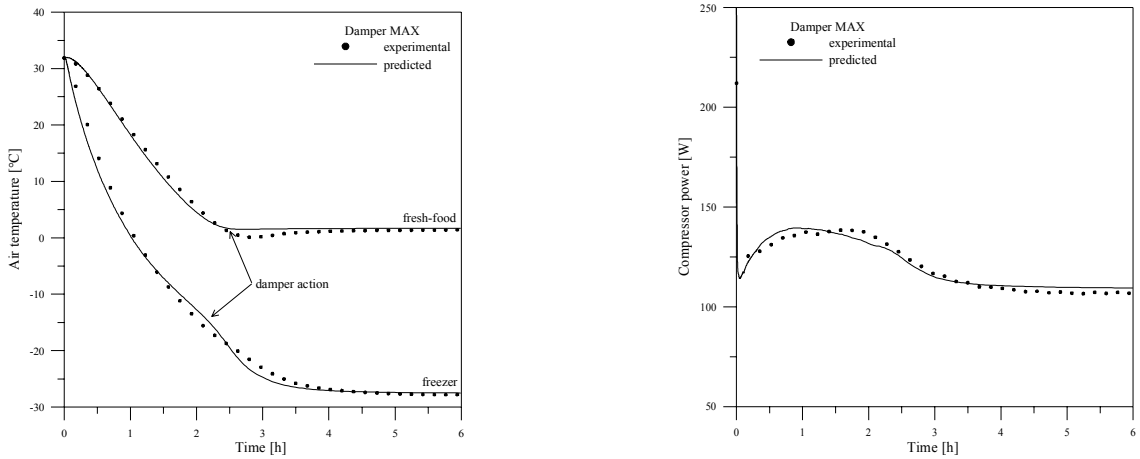

Figure 8: Start-up transients: air temperatures (*l*); compressor power (*r*)

Table 2: Average cycle comparisons

Thermostat-Damper	Energy consumption [kWh/month]			Running factor [dimensionless]			Fresh-food compartment temperature [°C]			Freezer compartment temperature [°C]		
	Sim.	Exp.	Dif.	Sim.	Exp.	Dif.	Sim.	Exp.	Dif.	Sim.	Exp.	Dif.
MIN-MIN	40.8	44.1	-7.6%	0.43	0.42	3.2%	11.6	10.8	0.8	-14.8	-15.7	0.9
MIN-MAX	49.0	51.4	-4.8%	0.52	0.50	3.2%	4.1	4.5	-0.4	-15.4	-16.5	1.1
MAX-MIN	48.3	53.2	-9.1%	0.54	0.56	-4.1%	11.5	10.4	1.1	-21.5	-21.9	0.4
MAX-MAX	61.2	62.9	-2.7%	0.68	0.66	2.4%	3.0	2.9	0.1	-22.2	-22.4	0.2

4. MODEL APPLICATION

The model was used to explore the influence of the capillary tube inner diameter and CT-LS HX effectiveness on the overall energy consumption. In all cases, the refrigerant charge was adjusted aiming at a minimum value for the energy consumption, while the average air temperatures were kept constant. The capillary tube diameter was changed from 0.655mm (current) to 0.6 and 0.7mm. As the tube diameter decreases, the refrigerant mass flow rate also decreases, and then more refrigerant is needed to preserve the cooling capacity, as shown in Fig.10*l*. At the same time the energy consumption also decreases with tube diameter. On the one hand, the time needed to fill the evaporator diminishes with tube diameter, improving the cooling capacity. On the other hand, the condensing pressure increases as the tube diameter decreases, increasing the compression power. As a net effect, the first overcomes the second, so the overall energy consumption decreases by 3.5% when the tube inner diameter is changed from 0.655 to 0.6mm. No significant change in the evaporation pressure was observed.

The influence of the CT-LS HX effectiveness was analyzed varying the heat exchanger length, but keeping the nominal dimensions of the capillary tube and suction line. Three configurations were studied: (i) short: L_e=1.898m, L_{hx}=0.622m; (ii) current: L_e=0.898m, L_{hx}=1.622m; and (iii) long: L_e=0.180m, L_{hx}=2.340m. Again, the refrigerant charge was adjusted since the vapor quality at the evaporator inlet, and therefore the required amount of refrigerant, decreases as the effectiveness increases. Fig.10*r* shows that the energy consumption decreases as the effectiveness increases, and this may be explained by the combined effect of the condensing pressure and cooling capacity. An overall energy consumption reduction of 5.5% was observed with configuration (iii).

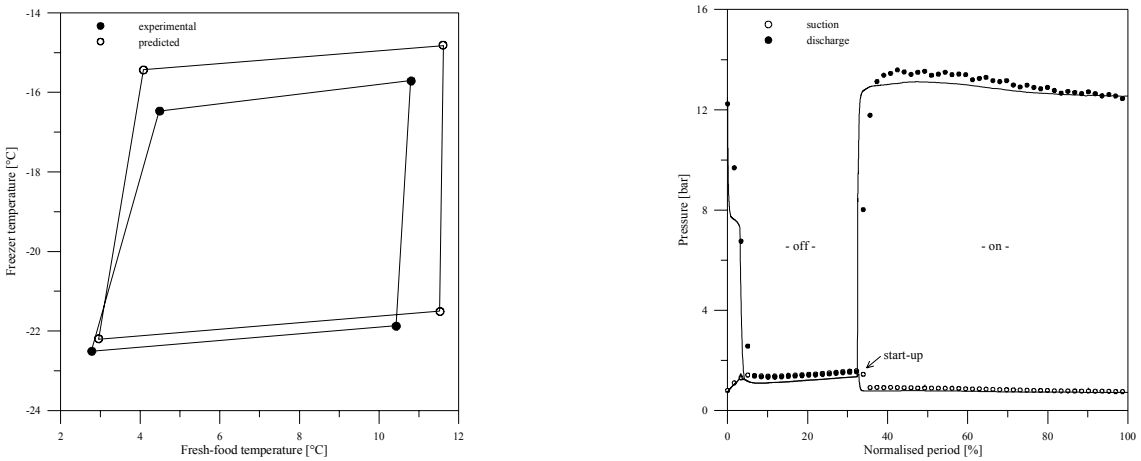

Figure 9: Cycling transients: control chart (*l*); suction and discharge pressures (*r*)

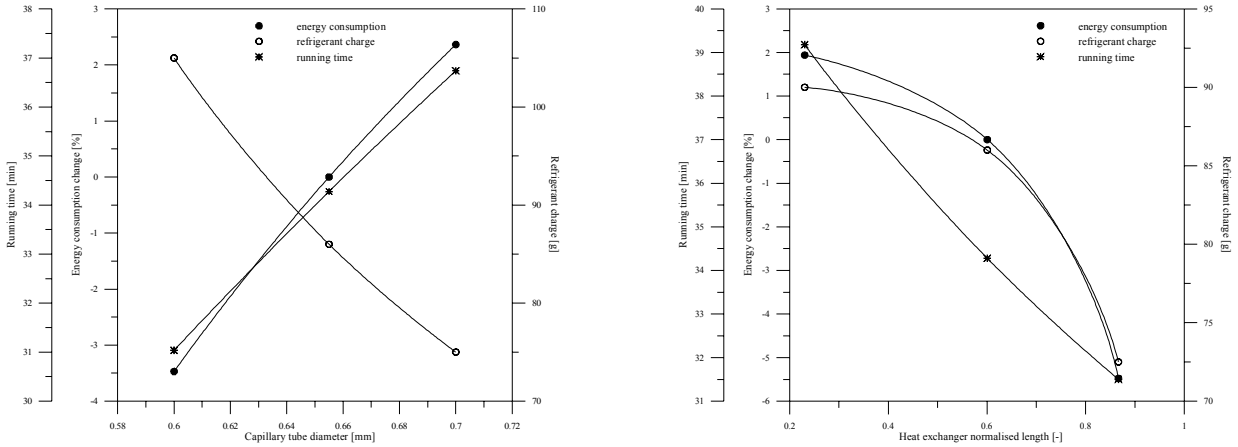

Figure 10: Model applications: effect of capillary diameter (*l*); effect of CT-LS HX heat exchanger effectiveness (*r*)

5. CONCLUDING REMARKS

A novel methodology for modeling and simulating the dynamic behavior of domestic refrigerators was proposed. Innovative features are incorporated into all component sub-models in order to guarantee both physical reliability and numerical robustness. Numerical predictions were compared to experimental data showing an excellent level of agreement for the whole range of operating conditions, including start-up and cycling regimes. The energy consumption and the air temperature maximum deviations from the experimental data were found to be ±10% and ±1°C, respectively.

The code was used to investigate the impact of the CT-LS HX geometry on the overall energy consumption of the system. It was found that the energy consumption can be reduced by 8%, by changing the capillary tube inner diameter to 0.6 mm and the heat exchanger length to 2.340m, with a refrigerant charge of 80g. The code predicts 12h of testing using only 30 minutes of CPU time (Pentium M 2.13GHz; 1024Mb RAM). Furthermore, the model can be easily adjusted to any kind of cabinet model.

REFERENCES

Baroczy, C.J., 1965, Correlation of liquid fraction in two-phase flow with application to liquid metals, *Chem. Eng. Prog.*, 61 (57), 179-191

Chi, J., Didion, D., 1982, A simulation model of the transient performance of a heat pump, *Int. J. Ref.*, 5(3), 176-184

Cyphers, J.A., Cess, R.D., Somers, E.V., 1958, Heat transfer character of wire-and-tube heat exchangers, *ASHRAE Semiannual Meeting*, New Orleans, LA, USA, 86-90

Domanski, P.A., 1991, Simulation of an evaporator with non-uniform one-dimensional air distribution, *ASHRAE Trans. Symposia*, 793-802

Fauske, H.K., 1962, Contribution to the theory of the two-phase, one component critical flow, *Internal Report, Argonne National Laboratory*, Argonne, USA

Gnielinski, V., 1976, New equations for heat and mass transfer in turbulent pipe and channel flow, *Int. Chem. Eng.*, 16, 359-368

Hermes, C.J.L., 2006, A novel methodology for dynamic simulation of domestic refrigerators, *PhD thesis*, Federal University of Santa Catarina, Florianópolis, Brazil, 272p. (in Portuguese)

Jakobsen, A., 1995, Energy optimisation of refrigeration systems: the domestic refrigerator – a case study, *PhD thesis*, Technical University of Denmark, Lyngby, Denmark

Jansen, M.J.P., Kuijpers, L.J.M., de Wit, J.A., 1988, Theoretical and experimental investigation of a dynamic model for small refrigerating systems, *IIR/IIF Meeting at Purdue*, 245-255

Jung, D., Song, K.-H., Cho, Y., Kim, S.-J., 2003, Flow condensation heat transfer coefficients of pure refrigerants, *Int. J. Ref.*, 26, 4-11

Karatas, H., Dirik, E., Derbentli, T., 1996, An experimental study of air-side heat transfer and friction factor correlations on domestic refrigerator finned-tube evaporators coil, *Int. Ref. Conf. at Purdue*, 465-470

Lee, T.-H., Lee, J.-S., Oh, S.-Y., Lee, M.-Y., Lee, K.-S., 2002, Comparison of air-side heat transfer coefficients of several types of evaporators of household freezer/refrigerators, *Int. Ref. Conf. at Purdue*, R16-5

MacArthur, J.W., 1984, Transient heat pump behaviour: A theoretical investigation, *Int. J. Ref.*, 7 (2), 123-132

Melo, C., Ferreira, R.T.S., Negrão, C.O.R., Pereira, R.H., 1988, Dynamic behaviour of a vapour compression refrigerator: a theoretical and experimental analysis, *IIR/IIF Meeting at Purdue*, West Lafayette, USA, 98-106

Papanek, W.J., Witzell, O.W., Fontaine, W.E., 1959, Convective films evaluated for wire and tube heat exchanger, *ASHRAE Journal*, June, pp.35-37

Ploug-Sørensen, L., Fredsted, J.P., Willatzen, M., 1997, Improvements in the modelling and simulation of refrigeration systems: aerospace tools applied to a domestic refrigerator, *J. HVAC&R Research*, 3 (4), 387-403

Prata, A.T., Ferreira, R.T.S., Fagotti, F., Todescat, M.L., 1994, Heat transfer in a reciprocating compressor, *Int. Comp. Eng. Conf. at Purdue*, West Lafayette, USA, 605-610

Rossi, T., Braun, J.E., 1999, A real-time transient model for air conditioners, *Int. Cong. Ref.*, Sydney, Australia

Tanda, D.W., Tagliafico, L., 1997, Radiation and natural convection heat transfer from wire-and-tube heat exchangers in refrigeration appliances, *Int. J. Ref.*, Vol.20, No.7, 461-469

Wongwises, S., Disawas, S., Kaewon, J., Onurai, C., 2000, Two-Phase Evaporative Heat Transfer Coefficients of Refrigerant HFC-134a Under Forced Flow Conditions in a Small Horizontal Tube, *Int. Comm. Heat & Mass Transfer*, 27 (1), 35-48

Yashar, D.A., Newell, T.A., Chato, J.C., Graham, D.M., Kopke, H.R., Wilson, M.J., 2001, An investigation of refrigerant void fraction in horizontal, microfin tubes, tubes, *J. HVAC&Research*, 7 (1), 67-82

Yasuda, H. Touber, S., Machielsen, C.H.M., 1983, Simulation model of a vapour compression refrigeration system, *ASHRAE Trans.*, 89 (2), 408-425

NOMENCLATURE

A	Area, m^2	L	Length, m	V	Volume, m^3		
C	Thermal capacity, W	M	Mass, kg	v	Specific volume, $m^3\ kg^{-1}$		
c	Specific heat, $J\ kg^{-1}\ K^{-1}$	p	Pressure, kPa	W	Power, W		
d	Diameter, m	Q	Heat transfer rate, W	w	Mass flow rate, $kg\ s^{-1}$		
G	Mass flux, $kg\ s^{-1}\ m^{-2}$	q	Heat flux, $W\ m^{-2}$	$\dot{y}$	Time-derivative (dy/dt)		
h	Specific enthalpy, $J\ kg^{-1}$	T	Temperature, °C	η	Efficiency		
$\hbar$	Heat transfer coefficient, $W\ m^{-2}\ K^{-1}$	u	Specific internal energy, $J\ kg^{-1}$	ρ	Specific mass, $kg\ m^{-3}$		
k	Thermal conductivity, $W\ m^{-1}\ K^{-1}$	t	Time, s	σ	Solubility, dimensionless		
Indexes							
a	Surrounding air	f	Fin	k	k-th control volume	s	Suction
d	Discharge	i	Internal air	o	Oil, External air	t	Tube
e	Entrance	in	Inflow	r	Refrigerant	w	Wall

ACKNOWLEDGEMENTS

The authors are grateful to Multibrás S.A. Eletrodomésticos and Embraco Compressors S.A. for the technical and financial support. The financial support from CAPES Agency is also duly acknowledged. Thanks are also addressed to the National Institute of Standards and Technology, in particular to Dr. Piotr A. Domanski for hosting Dr. C. J. L. Hermes during his 1-year sabbatical, during which this work was partially carried out.